Tunable Anion Selective Transport through Mono-Layer Graphene and Hexagonal Boron Nitride

Mustafa Caglar,[†] Inese Silkina,[‡] Bertram T. Brown,[†] Alice L. Thorneywork,[†] Oliver J. Burton,[¶] Vitaliy Babenko,[¶] Stephen Matthew Gilbert,[§] Alex Zettl,[§] Stephan Hofmann,[¶] and Ulrich F. Keyser[*,†]

[†]Cavendish Laboratory, University of Cambridge, J.J. Thomson Avenue, Cambridge CB3 0HE, United Kingdom

[‡]Department of Materials Science and Metallurgy, University of Cambridge, Cambridge CB3 0FS, United Kingdom

[¶]Department of Engineering, University of Cambridge, Cambridge CB3 0FA, United Kingdom

[§]Department of Physics, University of California at Berkeley, Materials Sciences Division, Lawrence Berkeley National Laboratory, Kavli Energy NanoScience Institute at the University of California, Berkeley and the Lawrence Berkeley National Laboratory, Berkeley, CA 94720 U.S.A.

E-mail: ufk20@cam.ac.uk

Abstract

Membranes that filter selectively for both anions and cations are central to technological applications from clean energy generation to desalination devices. 2D materials have immense

1

potential as these ion selective membranes, due to their thinness, mechanical strength and tunable surface chemistry. However, currently only cation selective membranes have been reported. Here, we demonstrate controllable cation and anion selectivity of both mono-layer graphene and hexagonal boron nitride. In particular, we measure the ionic current through membranes grown by chemical vapour deposition containing well-known intrinsic defects, native to wet-transferred 2D materials. We observe a striking change from cation selectivity with monovalent ions to anion selectivity by controlling the concentration of multivalent ions and inducing charge inversion on the 2D membrane. Furthermore, we find good agreement between our experimental data and theoretical predictions from the Goldman-Hodgkin-Katz equation and use this model to quantify the selectivity through extraction of selectivity ratios. These tunable selective membranes conduct up to 500 anions for each cation and thus show potential for osmotic power generation.

Keywords

graphene, hBN, ion selective membranes, GHK, charge inversion, anion selective, tunable

The pressing global need to improve technologies for generating clean energy and water desalination has triggered a flurry of research into porous ion-exchange membranes. Within these technologies, semi-permeable membranes are used to separate two electrolytes and subsequently perform electrical, mechanical or chemical work on the ionic flow. For example, ion exchange membranes have been used as a component in electrodialysis and reverse osmosis (RO) processes[1] to desalinate and extract precious metal from waste water. Both processes, however, are non-equilibrium as they require water to be driven through the membrane either electrically or by pressure, which is energy intensive and thus limits their net output efficiency. Recent innovations in energy recovery systems decreased net energy consumption

for pressure-driven RO by doing work with pressurized outputs,[2] however developing more energetically-efficient processes are key to the future of these technologies.[3]

Emergent technologies such as pressure retarded osmosis and reverse electrodialysis minimise this problem even further by using a salinity gradient to drive ion flow, requiring no active fluid pumping. In both cases a low resistance membrane is essential,[4] however for reverse electrodialysis, a stack of both cation and anion selective membranes are required to generate power.[5] The performance of a membrane within these applications thus depends heavily on key metrics including thickness of the membrane, surface chemistry and pore distribution. Two-dimensional (2D) materials such as graphene and hexagonal boron nitride (hBN) can be tailored to meet many of these requirements, making them ideal candidates for use as 2D ion exchange membranes.[6] For example, their atomic thinness results in not only a decrease in resistance against fluid flux but an intrinsic flexibility. In the case of graphene, the purely carbon composition makes surface functionalization relatively straightforward.[7] Control over surface properties is of particular interest as selectivity of ion transport in 2D materials has been shown to arise predominantly due to extrinsic charging effects.[8–10] As such, changing the charge polarity of the membrane potentially allows for manipulation of the magnitude and charge specificity of the membrane selectivity. This could provide a route to the anion selective membranes required by power generation applications that are presently absent in the literature, in marked contrast to multiple previous demonstrations of cation selectivity.

A further challenge arises as, although some disagree with this notion,[11] it is almost universally accepted that introduction of pores are critical to facilitating ionic transport. This is required as pristine graphene is impermeable to atoms as small as helium.[12] While precisely fabricated pores are a popular choice for preparing porous membranes, the helium-ion or electron beam processes used to create the pores come with significant overheads in cost, time and yield.[13,14] Recently, however, selective transport has been demonstrated for chemical vapor deposited (CVD) membranes[8] which can be produced at scale and with

high throughput.[15–17] Transport here is due to the intrinsic 'native' defects occurring from the CVD growth processes[18] as well as those introduced in transfer stages, removing the necessity for arduous pore creation processes. Moreover, larger scale treatments for controlled expansion of intrinsic defects are under development.[19–21] To fully exploit these materials, however, further efforts toward characterization of the distribution of intrinsic defects and their contribution to selectivity is required, which is currently lacking.

Here, we show anion selective behavior in both mono-layer CVD graphene and mono-layer hexagonal boron nitride (hBN) suspended on aqueous media. We use CVD materials which, except for a standard wet transfer, are not further processed. Therefore, we are not deliberately introducing defects, but assessing transport across intrinsic defects alone. Our membranes are characterized using high resolution transmission electron microscopy (HRTEM), *in situ* Raman spectroscopy and by conductance measurements. We build a framework for studying ionic transport through defects by sealing 2D membranes onto quartz nanocapillaries[22] which are used to contact and manipulate the materials (Figure 1a). Electrical contact on both sides of the membrane allow current and voltage characteristics to be measured across the membrane from which selectivity can then be determined. We find that multivalent salts such as hafnium tetrachloride (HfCl$_4$) cause membranes to exhibit anion selectivity. This anion selectivity is most likely the effect of surface charge reversal[23–25] by the multivalent ion, with a change from negative to positive surface charge causing a change from cation to anion selectivity. Moreover, anion selectivity of the membrane is also observed in monovalent salts - systems previously shown to exhibit cation selective behavior - if a low background concentration of multivalent ions is added to the solution. We model membrane performance using Goldman-Hodgkin-Katz (GHK)[26] relations and provide a quantitative analysis of selectivity. There are stark differences in chemical makeup and electrical characteristics between graphene and hBN, therefore in studying transport across two monolayer materials, commonly observed phenomena indicate universality, supporting isolation of their cause to extrinsic factors. Finally, to demonstrate the relevance of our system for techno-

logical applications, we calculate key metrics to assess the performance of these selective membranes as applied ion exchange membranes.
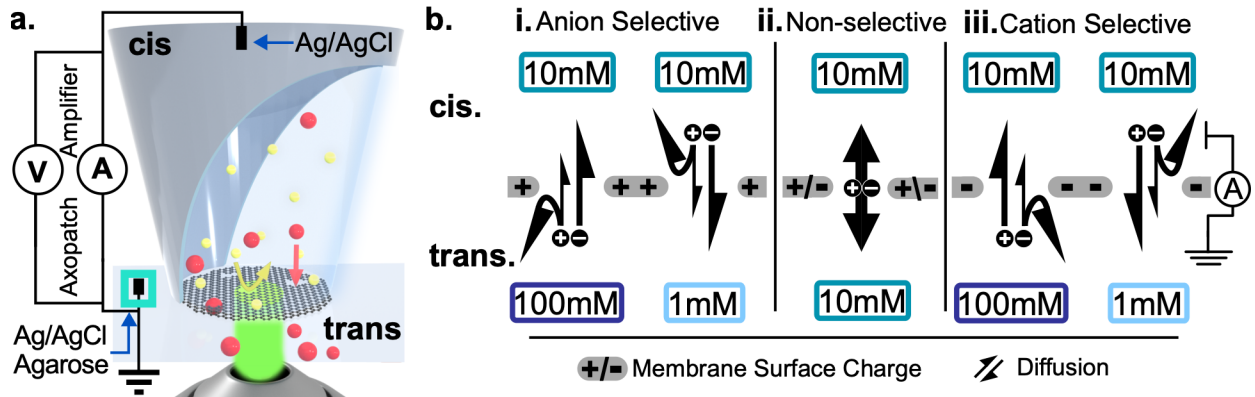
Results and discussion

Figure 1: Experimental setup and ion selectivity schematic for transport of ions through a charged membrane driven by a salinity gradient alone. (a) Saline solution filled quartz capillary in contact with an Ag/AgCl electrode with a graphene membrane sealed onto the tip. Opposing side of the membrane is another Ag/AgCl electrode coated in an agarose salt bridge. Ion rejection (yellow arrow) and selective transport (red arrow) by a nanopore in the graphene membrane is shown (not drawn to scale). (b) Selective drift current is measured for imposed concentration gradients across membranes with different surface charges. The net drift current is shown in each case with black arrows indicating the direction and magnitude of diffusive flow for: (i) an anion selective membrane; (ii) a membrane between reservoirs of equal concentration resulting in no net diffusive flux; and (iii) a cation selective membrane.

The method used to interface 2D membranes is described in *Experimental Methods* and summarized in brief in Figure 1a. A quartz nanocapillary (nominal diameter ∼150nm) is filled with saline solution and used to seal onto and pick up a piece of 2D material. The effect of the capillaries on ion selectivity is deemed negligible through a series of control experiments in the absence of a membrane.[8] *In situ* Raman (illustrated with a green laser) enables on-the-fly characterization of graphene. The capillary acts as a fixed cis reservoir which is then immersed into external trans reservoirs containing a variety of salts, exposing the sealed 2D material to distinct saline solutions. In order to establish membrane conductance and measure ionic transport, an amplifier is connected across the membrane using silver-

silver/chloride electrodes. With this, voltages can be applied, and current monitored across the membrane and *vice versa*. Conductance of the capillary without the membrane is used to establish the size of the nanometer opening of the capillary and the subsequent change in conductance upon contact with the 2D material gives an indication of the adherence of a 2D material on the capillary.

Transport across the 2D materials depends on the surface functionalization and charge, both termed extrinsic effects. Electrostatic charging of the surfaces of 2D materials on water has been demonstrated with estimates for graphene on water[13] as -0.6 C/m² and -0.16 C/m² for hBN.[27] Such extrinsic charging on both materials is most likely due to hydroxide adsorption[28] and this surface charge will determine the behavior of the nanopore with respect to its electrostatic interactions with ions in solution. In Figure 1b we illustrate the expected scenarios for ion flow through a charged semi-permeable membrane separating two ionic solutions, analogous to the system in Figure 1a. Since diffusion drives ion flow down a salinity gradient, both cations and anions will tend to flow from a lower to higher concentration. However, an imposed concentration gradient across the selective membrane results in diffusive flow of predominately one type of ion. This net movement of either the cations or anions in the system results in the observation of a current, with the current thus directly reflecting the selective behavior of the membrane. Note that here, for no driving voltage or current, measured voltages and currents are a result of the selective flux of ions down their concentration gradient alone.

The selective current will result in a reversal potential, V_{rev}, forming across the membrane, governed by the Nernst equation,

$$V_{rev} = S\frac{RT}{zF}\ln\left(\frac{C_{\text{trans}}}{C_{\text{cis}}}\right) \tag{1}$$

where C_{trans}/C_{cis} are the concentrations in the trans/cis reservoirs respectively, R denotes the gas constant, T is temperature, z is ion valency, F is Faraday's constant and S is percentage

of selectivity. The reversal potential indicates the potential that must be applied across the membrane to oppose the selective flux of ions arising from a concentration gradient. From equation 1, a system which is perfectly selective (S=1) toward either the cation or anion in a monovalent species at 300K would have an absolute reversal potential of 59.5 mV per decade molar concentration ratio (M) (mV/log(M)). Note that, a perfectly selective membrane toward anions will be permeable for anions and impermeable toward cations. For most systems, the membrane will not be perfectly selective *i.e.* there will also be some flux of the counter-ion across the membrane that will reduce the measured current. Here, measurement of the reversal potential can be used to quantify how close the membrane reaches the perfectly selective case.

To explore this further, Figure 1b.i presents possible scenarios for transport across a charged membrane. A positive surface charge will result in a higher population of anions around the pore region and thus transport through the pore is more preferential to anions, with only a fraction of cations also flowing (black arrows). The amount of cation flux across this otherwise anion selective pore will depend on the pore's selectivity ratio. Based on this, a current measured with no applied driving potential would be positive when the cis concentration ([cis]) is less than the trans concentration ([trans]) and negative when [cis]>[trans]. The reversal potential, when the current is zero, should be negative for [cis]<[trans] and positive when [cis]>[trans]. Figure 1b.ii shows a pore with no salinity gradient across it, resulting in no net diffusive flow rendering the pore non-selective. In measurements using our system, the case of equal cis and trans concentrations that should correspond to no measured current is used as a calibration point. Finally, Figure 1b.iii considers the case of a negatively charged surface, which results in cation selective behavior. Applying similar logic, the negative surface charge will result in a higher population of cations around the pore, thus making their transport across the pore more likely. In this case when [cis]<[trans], the current will be negative and when [cis]>[trans] the current will be positive. Similarly, the reversal potential should be positive for [cis]<[trans] and negative when [cis]>[trans].

7

These scenarios thus outline how the drift current and the potential across the membrane resulting from the asymmetrical ion flow is a direct quantifier of selectivity.

Current-Voltage (IV) curves are measured for the system with different concentration gradients across the membrane. For each capillary, at least three I-V curves are recorded at each trans concentration, sampled at 10mV steps, which are subsequently averaged, with error bars representing the spread in the data, see *Experimental Methods*. An illustrated example of processing data from I-V curves to selectivity ratios is presented in SI, S1. To assess the degree of the selectivity, we extract the current and voltage intercepts from I-V curves for a fixed cis concentration. These are then presented as a function of trans concentration. The voltage intercepts are a direct measure of the built-up membrane potential, or reversal potential, as expressed by equation 1. In line with this equation we find a linear behavior of the reversal potential with changing trans concentration on a log-linear scale. Inspection of equation 1 shows that the slope of this line should be directly related to the percentage selectivity, S. As such, gradients of the linear fits are used to provide a measure of the selectivity as the change in reversal potential with concentration (mV/log[M]). The gradient of the current-concentration plot (nA/log[M]) confirms the direction of selectivity and provides an idea of the selective ionic flux across the pore(s). Here, a negative gradient in the plot of reversal voltage against [trans] corresponds to a positive selective current gradient (from the definition of conventional current), and thus indicates anion selectivity. The opposite behavior would be expected for cation selective membranes. The direction of these gradients directly establishes which ions are diffusing across the membrane whilst the magnitude of the gradient indicates the degree of this selectivity.

In Figure 2a. we explore the effect of a solution of $HfCl_4$ containing multivalent ions, on the selectivity of mono-layer graphene. Each line in the figure represented a different cis concentration for the same set of trans concentrations. Here, the negative gradient in the plot of voltage offset *versus* concentration, or voltage selectivity, (Figure 2a.i) shows that the membrane transport is dominated by chloride ions in all cases. We therefore find
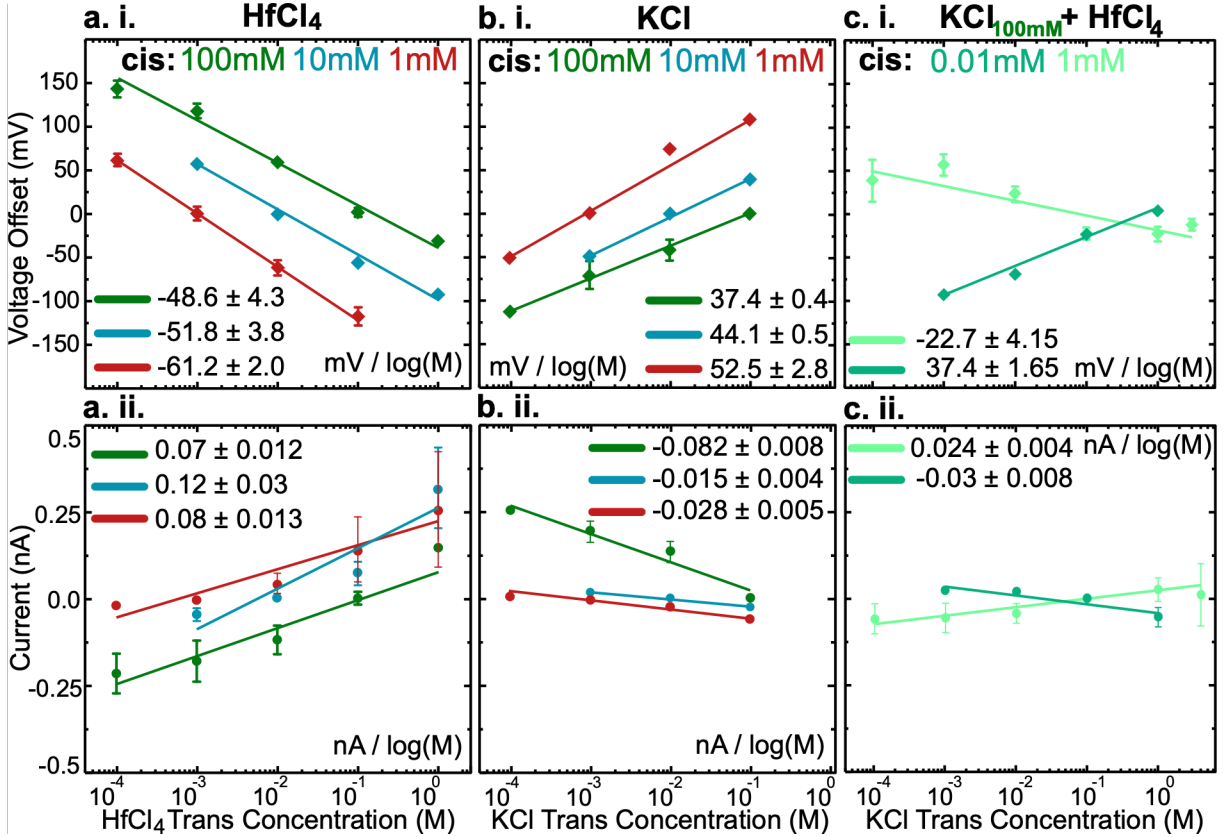
Figure 2: Tunable ion selectivity in different salt solutions. (a) $HfCl_4$ in cis and trans reservoirs, (a.i) the voltage offset as a function of trans concentration for different cis concentrations, all indicating anion selectivity. Gradients of each line are given in the legend with the largest magnitude gradient for [cis]= 1mM. The anion selective current (a.ii) is similar across all cis concentrations. (b) The corresponding data for KCl showing in all cases the expected cation selective behavior. (c) Voltage and current offsets for 100mM KCl with a low background concentration of $HfCl_4$ showing a change in the selectivity from cation to anion with increasing concentration of $HfCl_4$.

that anion selective transport dominates in a system with HfCl$_4$. Further, the magnitude of the slope - and thus the degree of anion selectivity - increases as the cis concentration decreases. From the extracted slopes and equation 1 the selectivity percentage, S, can be obtained. At 100mM and 10mM [cis], selectivity is at 82% and 88% of the theoretical maximum, respectively. Notably, selectivity reaches the theoretical maximum ($S=1$) for a cis concentration of 1mM. The current is further evidence of anion selectivity, however, here the magnitude appears to not depend significantly on cis concentrations. Note that the same behavior is seen with another tetravalent ionic solution, zirconium tetrachloride (ZrCl4), as shown in SI, S2. Moreover, hBN responds identically to that of graphene as shown in SI, S3. All salt solutions used are unbuffered with measured conductivities and pH values which are presented in SI, S4.

For comparison, in Figure 2b we show the equivalent behavior for cis and trans reservoirs filled with varying concentrations of KCl only. Here, as in previous reports,[7,9,13,29–32] transport is predominantly controlled by potassium ions and as such plots of the voltage offset *versus* trans concentration all have a positive gradient. As with HfCl$_4$, the magnitude of the slope increases with decreasing cis concentration although here the magnitudes are somewhat smaller than for the multivalent case. In particular, we observe at 100mM a selectivity of 64%, at 10mM, 75% and the highest selectivity of 90% ($S=0.9$) of the theoretical maximum for 1mM in the cis reservoir. Our result is consistent with other observations[8] which note that selectivity is largely controlled by the highest ion concentration as this alters the Debye screening length and thus the selectivity, which is yet another indication that the selectivity is due to extrinsic effects.

In light of the picture of selective transport outlined in Figure 1b, the contrasting behavior of the systems in Figure 2a and 2b suggests that while in the monovalent salt the membrane maintains a negative charge, with multivalent ions, the membrane instead develops a net positive charge. To further explore the effect of multivalent ions in positively charging the surface of the graphene, we now consider the effect on selective transport in

10

KCl of a small background concentration of $HfCl_4$. Figure 2c shows data from a system with 100mM KCl in the cis reservoir and varying KCl concentration in the trans reservoir with an addition of low concentrations of $HfCl_4$. With an addition of 0.01mM $HfCl_4$, cation selectivity is observed and at the same magnitude as seen without addition of $HfCl_4$ (green data in Figure 2b). Interestingly however, at an addition of 1mM $HfCl_4$ to 100mM KCl, a switch to anion selectivity is seen despite there being no gradient in $HfCl_4$ concentration across the system. Thus, chloride ion filtration is shown with KCl by use of a small but constant $HfCl_4$ background. The implication is that 1mM of $HfCl_4$ is sufficient to alter the graphene surface charge from negative to positive.[23,24] The mechanism by which this occurs is referred to as charge inversion[23,24] and, as an extrinsic process, is not a phenomena exclusive to 2D membranes. Furthermore, the reversibility of this inverting of surface charge, implies that the process is purely electrostatic as opposed to a surface chemical effect.

The crossover point from cation to anion selective behavior occurs between the addition of 0.1 and 1mM of $HfCl_4$. While the crossover concentration has previously not been determined for mixtures of monovalent and tetravalent ions, the crossover concentration in our experiments is consistent with that found for trivalent ions, where a crossover, or point of charge inversion, has been observed at $\sim$0.2mM.[24] Moreover, in repeating our experiment with trivalent salts, $CeCl_3$ and $LaCl_3$, we observe a point of charge inversion from cation to anion selectivity between 1mM - 10mM, with the decrease in value compared to that in the literature perhaps accounted for by differences between the inherent surface charge of the silica beads used in Dekker *et al.*[24] as opposed to the graphene surface used here, see SI, S5.

Considering concentration ratio, *i.e.* [cis]/[trans], across a range of fixed cis values, gives a more holistic overall view of performance. Furthermore, this allows for a selectivity ratio to be extracted from GHK equations as a function of concentration ratio and ionic valency alone. This parameter provides a more ready comparison of selective flux for systems for which the direction and magnitude of selectivity differ. The GHK equation describes ionic flux across a membrane as quantified by the transmembrane potential in terms of the ionic
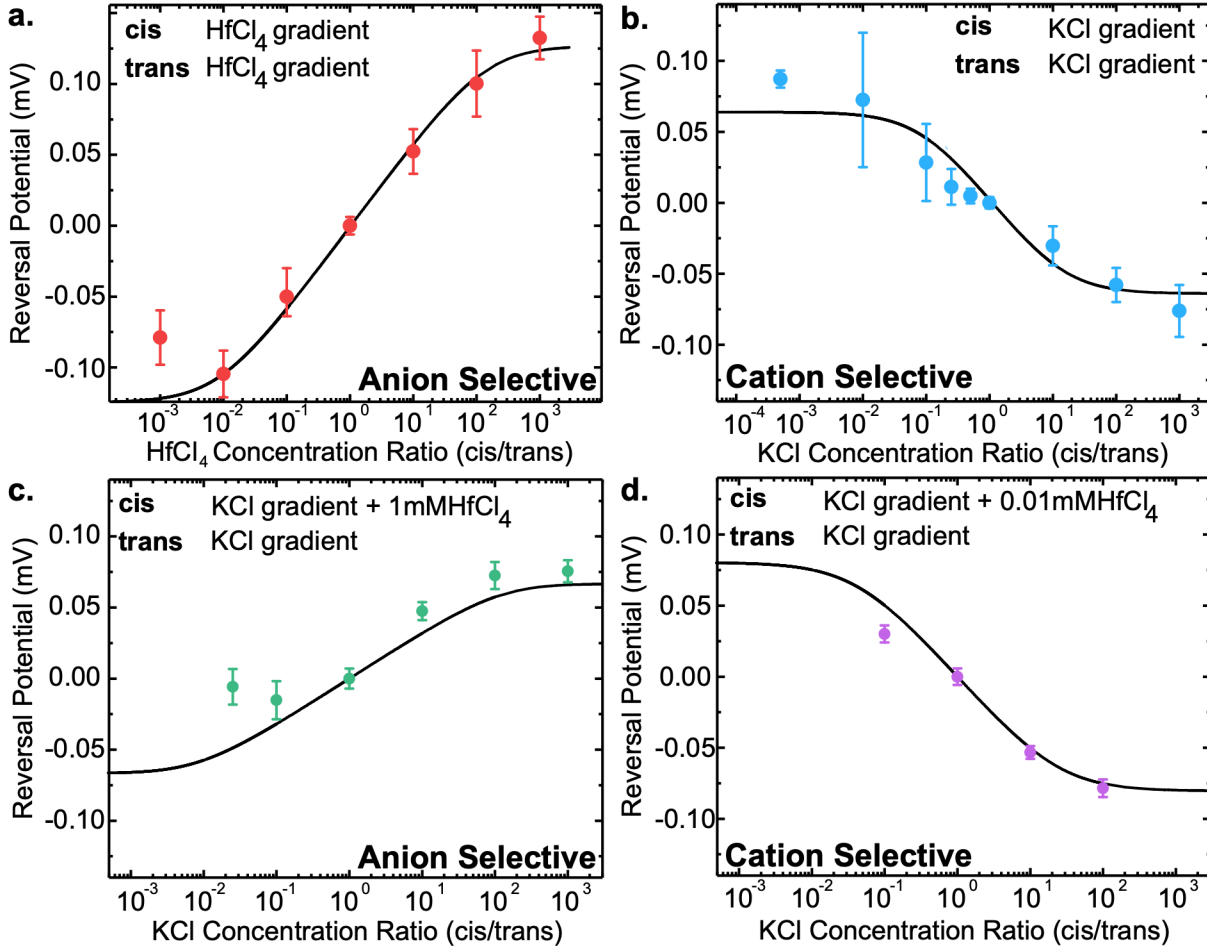
Figure 3: Selectivity ratio according to the GHK equation. Data from different cis concentration systems are combined and an overall GHK fit shown with the selectivity ratio as fitting parameter with experimental error shown as error bars. Legends indicate the salt in cis and trans (a) $HfCl_4$ is shown to be ~400 times more selective to anions over cations. (b) With KCl, the membrane is cation selective with a ratio of 12. (c) With the addition of 1mM $HfCl_4$ to KCl, the membrane is anion selective with a ratio of ~500 times more selective toward anions. (d) An addition of less $HfCl_4$ (0.01mM) preserved the cation selectivity seen with KCl, with a selective ratio toward cations of ~22.

concentration ratio and membrane selectivity ratio.[26] For the simplest case of a symmetric monovalent ion:

$$V_{\text{rev}} = \frac{RT}{F} \ln \left(\frac{P_{\frac{\text{cat}}{\text{an}}} + \frac{C_{\text{trans}}}{C_{\text{cis}}}}{P_{\frac{\text{cat}}{\text{an}}} - \frac{C_{\text{trans}}}{C_{\text{cis}}} + 1} \right) \qquad (2)$$

where R, F are molar gas and Faraday constants respectively, T temperature, C concentration and Pcat/an the selectivity ratio of cations relative to that of anions. In order to apply this model to multivalent ions an expanded form of the equation is used (see SI, S6). Figure 3 presents combined experimental data (symbols) for systems with monovalent, multivalent and mixtures of ions across a variety of cis/trans concentrations against the respective fit to the full GHK equation. Using nonlinear regression, the experimental values are fit to the GHK with the selectivity ratio (Pcat/an) as the only fitting parameter. This ratio is either quoted as Pcat/an or as its reciprocal, Pan/cat, for cation or anion selective systems respectively. While the GHK equation is based upon a number of assumptions (see SI, S6) the good level of agreement with our experimental data, suggests that this model provides a valid description of the underlying physical processes in our experiments. Overall, the experimental data for all systems is well modelled by applying GHK theory, which has been expanded to handle tetravalent ions. This implies that the transport observed adheres to electro-diffusion as described by Nernst-Planck (PNP) with the assumptions discussed in SI, S6.

Immediately clear is the striking contrast in GHK fit between $HfCl_4$ in Figure 3a and KCl in Figure 3b, supporting our findings of anion and cation selective behavior respectively. The magnitude of the selectivity ratio also differs between the systems. With $HfCl_4$, the system exhibits a selectivity ratio of 400 towards anions whereas this drops to 15 with KCl. The selectivity we observe for KCl is broadly consistent with other observations in literature.[8,13,33] From Figure 2a it can seen that by using $HfCl_4$, as opposed to KCl, the system exhibits increased selective ion flux at lower cis concentrations. This leads to an increase by an order of magnitude in ion selectivity compared to KCl, consistent with the fits shown here. The

magnitude of selectivity toward K^+ ions is maintained with the addition of 0.01mM $HfCl_4$ to a 100mM KCl cis reservoir (Figure 3c), not significantly affecting the selectivity ratio at 22. However, increasing the concentration of $HfCl_4$ to 1mM in Figure 3d, switches the selectivity to anion selective, despite the lack of a gradient of $HfCl_4$ across the system. Surprisingly, with the addition of the higher concentration of $HfCl_4$, the selectivity toward anions from a gradient of KCl is now an order of magnitude higher, at 500, compared to selectivity toward cations.

Having shown that by altering extrinsic charging effects we are able to tune ion selectivity across graphene and hBN we now address the mode of passage through the membranes. It has previously been implied that transport occurs *via* intrinsic defects.[8,34,35] In order to better assess these potential pathways, *in situ* Raman, high resolution transmission electron microscopy (HRTEM) and membrane conductance is used. These characterization methods with the exception of membrane conductance are more readily applied to graphene than for other 2D materials. However, here we assume that measuring similar membrane conductance data from both materials implies similar defect distributions as determined for graphene by other direct measures such as TEM and Raman spectroscopy. Figure 4a shows some typical Raman spectra for mono-layer graphene suspended on an electrolyte solution with different spectra coming from distinct graphene membranes on identical electrolyte - each spectrum is an accumulation of several repeated spectra. The spectra shows a prominent 2D peak at 2685 cm^{-1} and G peak at 1597 cm^{-1}, the intensity ratio of which is ~2.1, indicative of a monolayer sample.[36] The presence of the D peak at 1347 cm^{-1} is indicative of defects within graphene with further characterization of graphene and hBN in SI, S7. Defects could take the form of large cracks or a collection of smaller scale defects referred to as edge defects. Given the nature of how the material is both fabricated and characterized, this peak is most likely attributed to a collection of smaller scale edge defects.[36] Although the graphene used in this paper is single crystal monolayer, we do not imply an absence of defects. In fact, CVD-grown material as used here has been shown to have as high mobilities as 'pristine'
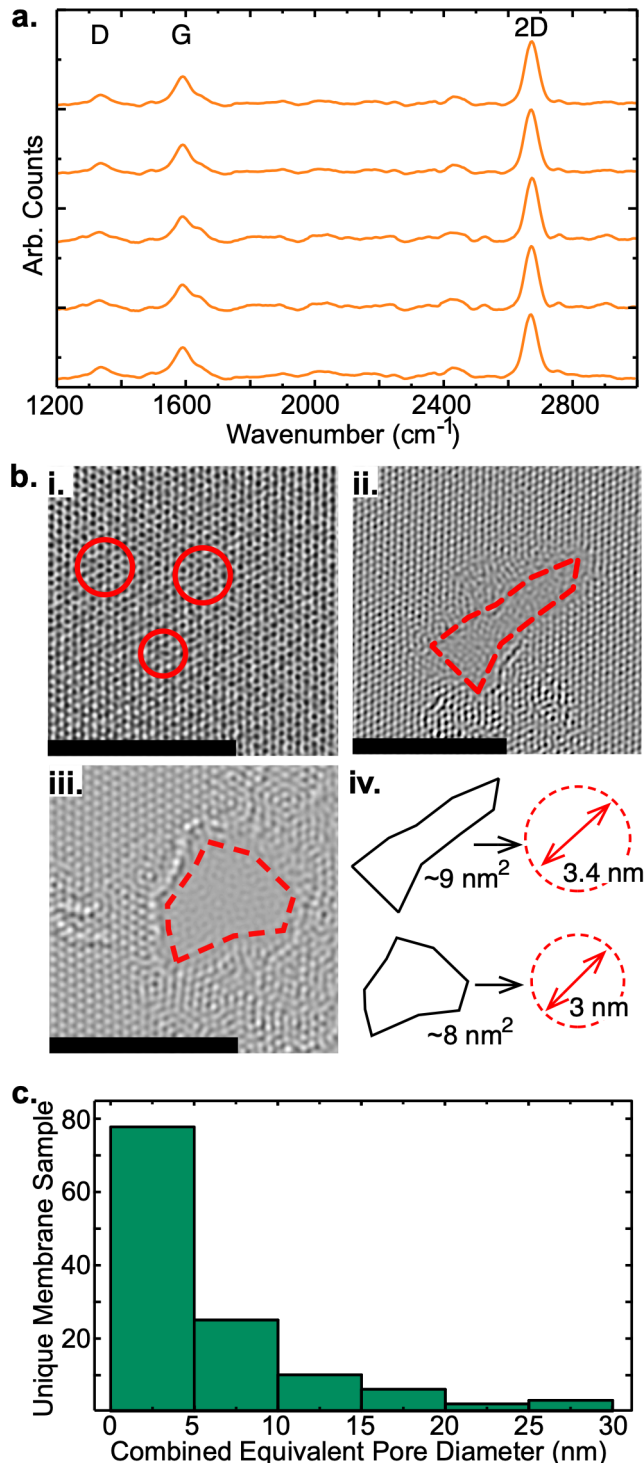
Figure 4: Membrane and pore characterization in graphene. (a) Raman spectra showing prominent 2D (2685 cm^{-1}), G (1597 cm^{-1}) and D (1347 cm^{-1}) peaks with a 2D:G intensity ratio of 2.1, indicative of defected mono-layer graphene. Raman was captured *in situ* with graphene suspended on a salt solution. Shown is multiple spectra taken at different points for a sample of graphene floating on KCl. (b) Post exit wave reconstruction HRTEM phase images showing various regions of the graphene sample, (i) Stone-Wales defects are circled, ii-iii show defected regions, iv. defected regions are shown to have areas equivalent to a ∼3nm circular pore. Scale bar, 5nm. (c) Distribution of summed total circular defect area which could account for experimentally observed selective currents.

exfoliated flakes.[37] As CVD materials usually have to be transferred, the most likely origin to intrinsic defects are due to standard wet-transfer methods as used here.

As defects within an otherwise impenetrable membrane provide the only pathway for charge to flow[38] further characterization of the intrinsic defects is important. To this end high resolution transmission electron microscopy (HRTEM) is used on graphene samples prepared identically to those used in experiments. Some representative post exit wave reconstructed images (SI, S8) are shown in Figure 4b Figure 4b.i shows an area of graphene where the hexagonal order of the lattice is seen alongside single atomic vacancy defects and some lattice disordering, referred to as Stone-Wales defects (red circles). These defects are, however, too small to account for selective ionic transport.[9] Figure 4b.ii-iii show examples of larger intrinsic defects which could facilitate selective ionic transport. The area of these defects are $\sim$8-9 nm^2, corresponding to an equivalent diameter of $\sim$3nm for a circular defect as shown in Figure 4b.iv.

High resolution microscopy is a powerful tool but only provides a limited view, making the extraction of large-scale statistics for the material difficult. Furthermore, it should be noted that TEM imaging is not carried out *in situ* and thus is not a direct characterization of defects through which we measure selective currents but instead is a characterization of the membrane as identically used in selectivity measurements. Therefore, both for a larger scale and more direct quantification of such defects, an empirical approach based on the membrane conductivity is used. The conductivity is measured by taking the resistance from I-V curves for a fixed salt concentration and fixed membrane area. The contributing resistance from the capillary is subtracted, see SI,S9, from this to leave the conductivity of the membrane alone. Unlike TEM, this approach considers the whole membrane area and thus provides an indication of the sum total defect area across the sample. To relate the conductivity of the membrane to the density of defects we first assume that we can approximate the conductivity through many smaller defects by that through a single larger pore with an area equal to the sum of the areas of all the individual defects. For a single circular pore, the

following empirical equation can be used to estimate the conductance as,[39]

$$G = \sigma \left(\frac{4t}{D^2} + \frac{1}{D} \right)^{-1} \tag{3}$$

where σ is the solution conductivity, t is the membrane thickness (taken as 0.6nm for graphene on water[39]) and D the pore diameter. From around 130 selective membrane samples, the conductance is measured and from this an estimate of the size of the pore that would be required to account for the observed conductance is determined from equation 3. In Figure 4c we plot the distribution of equivalent pore sizes for these samples. Over half of selective membrane samples show ionic flux accountable by defects of diameter 5nm or smaller which is consistent with the observed defects in the HRTEM images. Moreover around 75% of samples exhibit conductivities consistent with a total defect area equivalent to a 10nm diameter circular pore or smaller (see SI,S9 for a discussion on analysis). Having sealed onto a membrane, measurements of no appreciable conductance did not occur. Since pristine graphene is impermeable to ions and ionic conduction occurs through the sealed membrane exclusively - leakage around the rim of the capillary is negligible if present - we assume that the selective flux observed is through these defects, though the lack of experimental *in situ* imaging, means one can only infer that these pores are the selective current pathways.

Despite much recent literature providing theoretical and experimental evidence for selectivity within pores larger than that accountable by Debye overlap, notions that an obligatory condition for selectivity is that the Debye screening length in the system is comparable to the pore size still persist.[40–43] However in our experiments we observe selectivity in pores with an equivalent diameter of up to ∼30nm, in spite of Debye lengths that can be as short as ∼0.3nm for the monovalent electrolyte and ∼0.1nm for the tetravalent electrolyte[44](see SI, S10 for Debye screening lengths in our system). Due to how we measure conductance, the equivalent pore size could also be made up of many smaller defects, we note that based

on the selectivity we observe these singular defects should be smaller than 3nm.[8] If the selectivity we observe originates from larger pores, the observations would not be fully described by Debye overlap. Since the selectivity is not limited by the size of the ion, it is also not attributable to steric effects, see SI, S10. However, Poggioli *et al.*[45] have shown that surface conductance plays a key role in generating ion selectivity - a phenomenon governed by Dukhin length overlap. It is known that the surface conductance of 2D materials are heavily affected by their substrate[46–48] and in keeping with this, we see Raman spectra of graphene on various concentrations of KCl/$HfCl_4$, which show positive/negative shifts in 2D and G peaks indicating negative/positive surface charge respectively, refer to SI, S11. A full exploration of the Dukhin length in our system would require more careful characterization of the surface conductance, which is beyond the scope of this work. However, within this theoretical framework, selectivity has been previously demonstrated for pores measuring up to 100nm as reported by Rollings *et al.*[13] amongst others,[43,49] which would be consistent with our results. A key consequence of this is that the defects studied in this work could potentially be expanded (for example by ozone treatment[3,8,14] or chemical etching[8,50]) closer to 100nm whilst maintaining selectivity. This would increase the fluid flux through the pores, increasing selective flux and thus any potentially generated osmotic power using this system.

Finally, to assess the membrane performance for applications in power generation, in Figure 5 we show the selectivity ratios as a function of cis reservoir concentration, and a projection of the osmotic power generation for all considered systems. Here in Figure 5a, in contrast to Figure 3, the GHK derived selectivity is extracted and shown separately for each cis reservoir concentration (for individual analytical fits see SI, S12). Given that magnitude of selectivity is affected not just by the concentration ratio but also by the absolute value of the cis concentration, determination of the maximum obtainable selectivity ratio as opposed to the mean requires systems with different cis concentrations to be considered separately. Figure 5a also shows, once again, the striking change from a cation selective regime with KCl to an anion selective with $HfCl_4$, with a clear transition point in mixed environments.
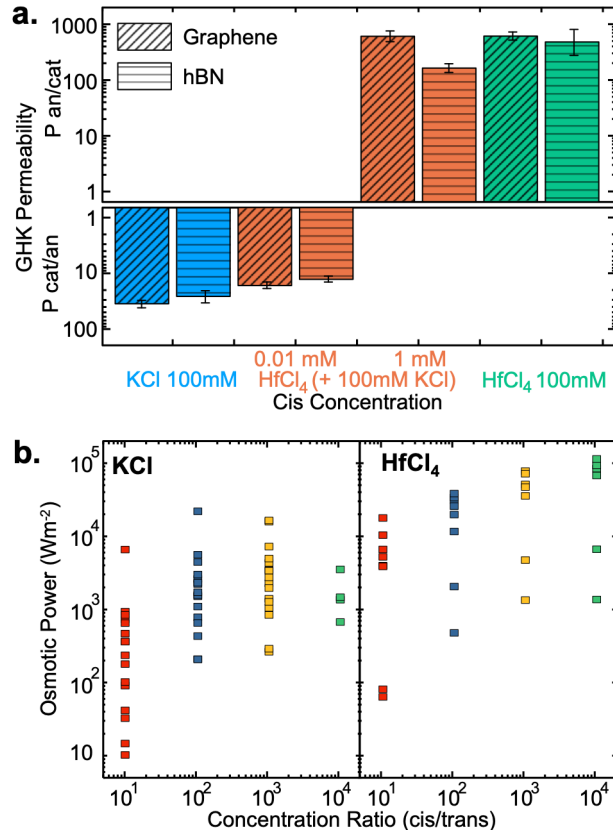
Figure 5: Selectivity ratios and power generation within our system. (a) KCl is shown as cation selective with a higher selectivity ratio for a cis concentration of 100mM. Addition of 0.01mM HfCl$_4$ maintains cation selectivity, however 1mM switches to anion selective. HfCl$_4$ is anion selective with a high selectivity ratio of around 500. Behavior for both graphene and hBN is shown, showing similar preference in both materials. (b) KCl and HfCl$_4$ power generation as a function of concentration ratio using graphene is compared. HfCl$_4$ can generate over 100kW/m2 whilst the figure is lower at 10kW/m2 with KCl.

The highest selectivity ratios are achieved in systems with 100mM in the [cis] reservoir. Importantly, it is clear that the performance of hBN is comparable to that of graphene. The insulating nature of hBN, reduced order of atomic symmetry and different chemical composition present it as a contrasting 2D material to graphene. Since the system with hBN responds in a way consistent with that of graphene, we can assume that the ionic transport phenomena is extrinsic to the 2D materials itself and is more dominated by the surface effects.

Within a would-be application such as the extraction of energy from ionic flux, Figure 5b presents the osmotic power that could be generated using our system. The osmotic power values we measure for KCl are nominally in the region of 10^3 W/m^2, peaking at 10^4 W/m^2 which agrees with previous calculations for a similar system.[8,49] Compared to KCl, the power extracted from HfCl$_4$ increases by 10-100 times; the significant increase as expected from the selectivity ratios shown in Figure 5a Reaching a peak of 10^5 W/m^2 potential osmotic power, this system compares favorably to performance in enlarged graphene defects and to commercial Nafion membranes.[8] Recently, using methods of enhancing transport through pores, Graf *et al.*[19] estimate extraction of 160pW per 10nm milled pores in MoS$_2$, which is on the order 10^5 W/m^2 (depending on the assumed pore distribution). Our system thus provides comparable power values and an increase seems possible if pores size and surface charge are optimised in future.

Conclusion

We have shown that multivalent ions can be used to alter surface charge on 2D membranes allowing for tunable anion/cation selectivity. By measuring the current across membranes sealed onto glass nanocapillaries in a variety of salt conditions the magnitude and direction of selectivity has been established. As extrinsic charge effects are known to significantly influence the selectivity across 2D membranes, this suggests that the negative charge on the

2D membrane surface and thus around the pore, is altered by multivalent ions such that transport of anions is preferential to cations. We find that this effect can be induced in monovalent salts by the addition of a multivalent salt. The immediate implication is that the magnitude and direction of ion selectivity can be controlled and tuned extrinsically. The development of anion selective membranes is a crucial step in furthering understanding of surface charge interactions as well as allowing for direct application in cation / anion selective stacked systems. Thus, our finding provides potential for the use of 2D materials as IEMs. We infer that selective transport in our system could be due to pores similar to imaged defects intrinsic to transferred CVD membranes, removing the requirement for laborious pore creation techniques. We imaged defects for as - grown graphene being on the order of ~3nm and that even for these relatively small defects, correlated selectivity to membrane conductance, shows that a high level of selective salt permeability can be achieved coupled with lower fluid resistance. Anion selectivity is found to persist at high salt concentrations, increasing the potential osmotic power generated using these systems. Moreover, we have shown that lower conductance membranes and thus those with enlarged defects, could remain selective and so provide even lower fluid resistance. As such, moving forward, surface treatments allowing for the defects to be enlarged up to 100nm, increasing the ionic flux across the membranes, would make these systems even more attractive in technological applications. Moreover, *in situ* high resolution imagery with live selectivity experiments would directly characterize pores and correlate that with an associated selectivity, further elucidating selective current pathways in 2D membranes.

Experimental Methods

Graphene Preparation

Monolayer graphene was produced in a cold walled CVD reactor (AIXTRON BM Pro 4) using 99.8% 25um thick copper foil (Alfa-Aesar) as a catalyst. The copper was cleaned in

acetone and IPA before being partially oxidized prior to synthesis. The synthesis procedure consisted of annealing at 1070 C in 50mbar of argon for 30 minutes before being exposed to 50mbar of 4000:1000:1 Ar:H2:CH4 gas mixture for 90 minutes resulting in full coverage of the copper foil by graphene (>99% monolayer, grain-size >100um[51]) - confirmed by Raman (Renishaw inVia) and SEM (FEI Magellan 400) respectively, see SI,S7.

Hexagonal Boron Nitride Preparation

hBN material was grown similarly to the methods reported previously.[52] Briefly, iron foils (100 m, Goodfellow, 99.8%) were cleaned in acetone and IPA and loaded into a custom cold-wall CVD system with a graphite heater. The temperature was ramped to 940 °C at 50 °C/min and the foils were annealed in ammonia atmosphere (4 mbar, 5 minutes). For hBN synthesis, borazine was added as a precursor ($1e^3$ mbar, 5 minutes) and the system was rapidly cooled (200 °C/min initially) by turning off the heater. An electrochemical bubbling transfer method[53] was used to deposit hBN films onto SiO2 substrates for Raman characterisation. See SI for further details and characterization.

Membrane Transfer

For graphene grown on copper as described, a PMMA supporting layer is used to etch the copper using ammonium persulfate and the subsequent PMMA-graphene layer is transferred onto to cleaved KCl chips. Acetone and IPA washes are used to remove PMMA. Meanwhile for hBN a PMMA free method involving an electrochemical process[53] is used to cleave onto KCl chips. Finally, gold strips are evaporated through a shadow mask onto the graphene/hBN to serve as optical guiding lines and a supporting framework.

Fluidic cell preparation

Quartz capillaries (Sutter) with 0.5mm/0.3mm (inner/outer) diameter were sonicated in ethanol for 10 minutes before drying under a nitrogen stream and baking at 60°C to remove residual ethanol. Capillaries are pulled to a nominal inner diameter of 150nm using a laser assisted puller (Sutter P-2000). Expected morphology and pore diameter are confirmed by SEM see SI for images and pore size distribution. Back end of capillaries are submerged in to desired salt solution and placed in a vacuum desiccator to induce capillary filling. Filled capillaries are inserted into a holder (Axopatch Holder with Suction Port) which can be mounted into an Axopatch head-stage.

Ion selectivity measurements

The experimental setup is shown in Figure 1a. Graphene and other 2D membranes are contacted using quartz capillaries with a 150nm circular opening. The capillaries are first filled with a salt solution forming the cis chamber. This is then sealed by a 2D material, forming a free-standing structure. The sealed capillary is exposed to different external salt solutions forming the trans reservoir. Thus, the material is exposed to a fixed salt in the capillary and a variable trans salt, allowing for the introduction of a salt concentration gradient across the membrane. Disposable Ag/AgCl electrodes are made by submerging pure silver wire in sodium hypochlorite for at least 1 hour. Electrodes are placed on either side of the graphene membrane, one in the capillary holder (cis) and the other is exposed to a salt solution (trans). In order to eliminate REDOX potentials[54] due to salinary gradients at the trans electrode, a matched agarose salt bridge is used. The electrodes are connected to the head-stage of an Axopatch 200B patch clamp amplifier (Molecular Devices). All current measurements were subject to an internal amplifier Bessel filter at 10 kHz, recording at 20 kHz - each current step is recorded for 1 second with a 500 ms settling time. Preceding selectivity measurements, the amplifier voltage offset is calibrated using symmetric salt conditions. DC voltages are applied in steps of 20mV from up to -200mV to 200mV and the current measured.

Data Analysis

Multiple I-V curves are recorded for each data point, these are averaged and a standard error extracted. A linear fit is then applied to the I-V measurements, extracting reversal potentials and leakage currents. A plot of the reversal potentials and leakage currents against the trans concentration is used to extract the gradient of a linear fit, exposing measures of selectivity. Additionally, the measured reversal potentials are used to estimate ion selectivity according to the expanded GHK equation (SI, S6) using nonlinear regression, standard errors are used as weights in the regression with a standard error found for the fitting parameter.

Imaging

High resolution TEM (HR-TEM) imaging was taken using the TEAM 0.5 microscope at Lawrence Berkeley National Laboratory. This microscope achieves high resolution through spherical aberration correction and a monochromatic beam. The microscope was operated at 80 kV to prevent knock-on damage of the graphene sample. Through focal series images were taken from -50 to 50 nm about the focal plane. Exit wave reconstruction (see SI, S8) is used for the through focal series to produce HR-TEM images.

Acknowledgement

Supporting Information Available

Detailed example of the analysis used, derivations of GHK model equations, experimental data on divalent, trivalent and other tetravalent ions, discussion with experimental data on pH considerations within the system, material characterisation data and further Raman spectra are presented within the Supporting Information. This material is available free of charge *via* the Internet at `http://pubs.acs.org`.

References

1. Varcoe, J. R.; Atanassov, P.; Dekel, D. R.; Herring, A. M.; Hickner, M. A.; Kohl, P. A.; Kucernak, A. R.; Mustain, W. E.; Nijmeijer, K.; Scott, K.; Xu, T.; Zhuang, L. Anion-Exchange Membranes in Electrochemical Energy Systems. *Energy Environ. Sci.* **2014**, *7*, 3135–3191.

2. Ghaffour, N.; Missimer, T. M.; Amy, G. L. Technical Review and Evaluation of the Economics of Water Desalination: Current and Future Challenges for Better Water Supply Sustainability. *Desalination* **2013**, *309*, 197–207.

3. Aliprandi, A.; Pakulski, D.; Ciesielski, A.; Samorì, P. Punctured Two-Dimensional Sheets for Harvesting Blue Energy. *ACS Nano* **2017**, *11*, 10654–10658.

4. Luo, T.; Abdu, S.; Wessling, M. Selectivity of Ion Exchange Membranes: A Review. *J. Membrane. Sci.* **2018**, *555*, 429–454.

5. Kim, D. K.; Duan, C.; Chen, Y. F.; Majumdar, A. Power Generation from Concentration Gradient by Reverse Electrodialysis in Ion-Selective Nanochannels. *Microfluid. Nanofluid.* **2010**, *9*, 1215–1224.

6. Sahu, S.; Zwolak, M. Colloquium : Ionic Phenomena in Nanoscale Pores through 2D Materials . *Rev. Mod. Phys.* **2019**, *91*, 21004.

7. Hong, S.; Constans, C.; Surmani Martins, M. V.; Seow, Y. C.; Guevara Carrió, J. A.; Garaj, S. Scalable Graphene-Based Membranes for Ionic Sieving with Ultrahigh Charge Selectivity. *Nano Lett.* **2017**, *17*, 728–732.

8. Walker, M. I.; Ubych, K.; Saraswat, V.; Chalklen, E. A.; Braeuninger-Weimer, P.; Caneva, S.; Weatherup, R. S.; Hofmann, S.; Keyser, U. F. Extrinsic Cation Selectivity of 2D Membranes. *ACS Nano* **2017**, *11*, 1340–1346.

9. Cohen-Tanugi, D.; Grossman, J. C. Water Desalination across Nanoporous Graphene. *Nano Lett.* **2012**, *12*, 3602–3608.

10. Kang, Y.; Zhang, Z.; Shi, H.; Zhang, J.; Liang, L.; Wang, Q.; Ågren, H.; Tu, Y. Na+ and K+ Ion Selectivity by Size-Controlled Biomimetic Graphene Nanopores. *Nanoscale* **2014**, *6*, 10666–10672.

11. Mogg, L.; Zhang, S.; Hao, G.-P.; Gopinadhan, K.; Barry, D.; Liu, B. L.; Cheng, H. M.; Geim, A. K.; Lozada-Hidalgo, M. Perfect Proton Selectivity in Ion Transport through Two-Dimensional Crystals. *Nat. Commun.* **2019**, *10*, 4243.

12. Bunch, J. S.; Verbridge, S. S.; Alden, J. S.; van der Zande, A. M.; Parpia, J. M.; Craighead, H. G.; McEuen, P. L. Impermeable Atomic Membranes from Graphene Sheets. *Nano Lett.* **2008**, *8*, 2458–2462.

13. Rollings, R. C.; Kuan, A. T.; Golovchenko, J. A. Ion Selectivity of Graphene Nanopores. *Nat. Commun.* **2016**, *7*, 11408.

14. O'Hern, S. C.; Boutilier, M. S. H.; Idrobo, J. C.; Song, Y.; Kong, J.; Laoui, T.; Atieh, M.; Karnik, R. Selective Ionic Transport through Tunable Subnanometer Pores in Single-Layer Graphene Membranes. *Nano Lett.* **2014**, *14*, 1234–1241.

15. Zurutuza, A.; Marinelli, C. Challenges and Opportunities in Graphene Commercialization. *Nat. Nanotechnol.* **2014**, *9*, 730–734.

16. Lin, L.; Peng, H.; Liu, Z. Synthesis Challenges for Graphene Industry. *Nat. Mater.* **2019**, *18*, 520–524.

17. Kobayashi, T.; Bando, M.; Kimura, N.; Shimizu, K.; Kadono, K.; Umezu, N.; Miyahara, K.; Hayazaki, S.; Nagai, S.; Mizuguchi, Y.; Murakami, Y.; Hobara, D. Production of a 100-m-Long High-Quality Graphene Transparent Conductive Film by Roll-to-Roll Chemical Vapor Deposition and Transfer Process. *Appl. Phys. Lett.* **2013**, *102*, 1–5.

18. Chin, H. T.; Lee, J. J.; Hofmann, M.; Hsieh, Y. P. Impact of Growth Rate on Graphene Lattice-Defect Formation within a Single Crystalline Domain. *Sci. Rep-UK.* **2018**, *8*, 3–8.

19. Graf, M.; Lihter, M.; Unuchek, D.; Sarathy, A.; Leburton, J.-P.; Kis, A.; Radenovic, A. Light-Enhanced Blue Energy Generation Using MoS_2 Nanopores. *Joule* **2019**, *3*, 1549–1564.

20. Koenig, S. P.; Wang, L.; Pellegrino, J.; Bunch, J. S. Selective Molecular Sieving through Porous Graphene. *Nat. Nanotechnol.* **2012**, *7*, 728–32.

21. Rabchinskii, M. K.; Shnitov, V. V.; Dideikin, A. T.; Aleksenskii, A. E.; Vul, S. P.; Baidakova, M. V.; Pronin, I. I.; Kirilenko, D. A.; Brunkov, P. N.; Weise, J.;

Molodtsov, S. L. Nanoscale Perforation of Graphene Oxide during Photoreduction Process in the Argon Atmosphere. *J. Phys. Chem. C* **2016**, *120*, 28261–28269.

22. Walker, M. I.; Weatherup, R. S.; Bell, N. A. W.; Hofmann, S.; Keyser, U. F. Free-Standing Graphene Membranes on Glass Nanopores for Ionic Current Measurements. *Appl. Phys. Lett.* **2015**, *106*, 23119.

23. Besteman, K.; Zevenbergen, M. A. G.; Lemay, S. G. Charge Inversion by Multivalent Ions: Dependence on Dielectric Constant and Surface-Charge Density. *Phys. Rev. E* **2005**, *72*, 1–9.

24. Dekker, C.; Besteman, K.; van der Heyden, F. H. J.; Stein, D.; Lemay, S. G. Charge Inversion at High Ionic Strength Studied by Streaming Currents. *Phys. Rev. Lett.* **2006**, *96*, 1–4.

25. Besteman, K.; Zevenbergen, M. A. G.; Heering, H. A.; Lemay, S. G. Direct Observation of Charge Inversion by Multivalent Ions as a Universal Electrostatic Phenomenon. *Phys. Rev. Lett.* **2004**, *93*, 4–7.

26. Hille, B. *Ionic Channels of Excitable Membranes*; Sinauer Associates: Sunderland, Ma, 2001; pp 450–460.

27. Weber, M.; Koonkaew, B.; Balme, S.; Utke, I.; Picaud, F.; Iatsunskyi, I.; Coy, E.; Miele, P.; Bechelany, M. Boron Nitride Nanoporous Membranes with High Surface Charge by Atomic Layer Deposition. *ACS Appl. Mater. Inter.* **2017**, *9*, 16669–16678.

28. Grosjean, B.; Bocquet, M. L.; Vuilleumier, R. Versatile Electrification of Two-Dimensional Nanomaterials in Water. *Nat. Commun.* **2019**, *10*, 1–8.

29. Sint, K.; Wang, B.; Král, P. Selective Ion Passage through Functionalized Graphene Nanopores. *J. Am. Chem. Soc.* **2008**, *130*, 16448–16449.

30. He, Z.; Zhou, J.; Lu, X.; Corry, B. Bioinspired Graphene Nanopores with Voltage-Tunable Ion Selectivity for Na$^+$ and K$^+$. *ACS Nano* **2013**, *7*, 10148–10157.

31. Zhao, Y.; Shi, W.; Van der Bruggen, B.; Gao, C.; Shen, J. Tunable Nanoscale Interlayer of Graphene with Symmetrical Polyelectrolyte Multilayer Architecture for Lithium Extraction. *Adv. Mater. Interfaces* **2018**, *5*, 1701449.

32. Sun, P.; Zheng, F.; Zhu, M.; Song, Z.; Wang, K.; Zhong, M.; Wu, D.; Little, R. B.; Xu, Z.; Zhu, H. Selective Trans-Membrane Transport of Alkali and Alkaline Earth Cations through Graphene Oxide Membranes Based on Cation-π Interactions. *ACS Nano* **2014**, *8*, 850–859.

33. Cantley, L.; Swett, J. L.; Lloyd, D.; Cullen, D. A.; Zhou, K.; Bedworth, P. V.; Heise, S.; Rondinone, A. J.; Xu, Z.; Sinton, S.; Bunch, J. S. Voltage Gated Inter-Cation Selective Ion Channels from Graphene Nanopores. *Nanoscale* **2019**, *11*, 9856–9861.

34. O'Hern, S. C.; Stewart, C. A.; Boutilier, M. S.; Idrobo, J. C.; Bhaviripudi, S.; Das, S. K.; Kong, J.; Laoui, T.; Atieh, M.; Karnik, R. Selective Molecular Transport through Intrinsic Defects in a Single Layer of CVD Graphene. *ACS Nano* **2012**, *6*, 10130–10138.

35. Jain, T.; Rasera, B. C.; Guerrero, R. J. S.; Boutilier, M. S.; O'Hern, S. C.; Idrobo, J. C.; Karnik, R. Heterogeneous Sub-Continuum Ionic Transport in Statistically Isolated Graphene Nanopores. *Nat. Nanotechnol.* **2015**, *10*, 1053–1057.

36. Ferrari, A. C.; Meyer, J. C.; Scardaci, V.; Casiraghi, C.; Lazzeri, M.; Mauri, F.; Piscanec, S.; Jiang, D.; Novoselov, K. S.; Roth, S.; Geim, A. K. Raman Spectrum of Graphene and Graphene Layers. *Phys. Rev. Lett.* **2006**, *97*.

37. De Fazio, D.; Purdie, D. G.; Ott, A. K.; Braeuninger-Weimer, P.; Khodkov, T.; Goossens, S.; Taniguchi, T.; Watanabe, K.; Livreri, P.; Koppens, F. H.; Hofmann, S.; Goykhman, I.; Ferrari, A. C.; Lombardo, A. High-Mobility, Wet-Transferred Graphene Grown by Chemical Vapor Deposition. *ACS Nano* **2019**, *13*, 8926–8935.

38. Celebi, K.; Buchheim, J.; Wyss, R. M.; Droudian, A.; Gasser, P.; Shorubalko, I.; Kye, J.-I.; Lee, C.; Park, H. G. Ultimate Permeation across Atomically Thin Porous Graphene. *Science* **2014**, *344*, 289–292.

39. Garaj, S.; Hubbard, W.; Reina, A.; Kong, J.; Branton, D.; Golovchenko, J. A. Graphene as a Subnanometre Trans-Electrode Membrane. *Nature* **2010**, *467*, 190–193.

40. Plecis, A.; Schoch, R. B.; Renaud, P. Ionic Transport Phenomena in Nanofluidics: Experimental and Theoretical Study of the Exclusion-Enrichment Effect on a Chip. *Nano Lett.* **2005**, *5*, 1147–1155.

41. Schoch, R. B.; Han, J.; Renaud, P. Transport Phenomena in Nanofluidics. *Rev. Mod. Phys.* **2008**, *80*, 839–883.

42. Ghosh, M.; Jorissen, K. F. A.; Wood, J. A.; Lammertink, R. G. H. Ion Transport through Perforated Graphene. *J. Phys. Chem. Lett* **2018**, *9*, 6339–6344.

43. Feng, J.; Graf, M.; Liu, K.; Ovchinnikov, D.; Dumcenco, D.; Heiranian, M.; Nandigana, V.; Aluru, N. R.; Kis, A.; Radenovic, A. Single-Layer MoS_2 Nanopores as Nanopower Generators. *Nature* **2016**, *536*, 197–200.

44. McBride, A.; Kohonen, M.; Attard, P. The Screening Length of Charge-Asymmetric Electrolytes: A Hypernetted Chain Calculation. *J. Chem. Phys.* **1998**, *109*, 2423–2428.

45. Poggioli, A. R.; Siria, A.; Bocquet, L. Beyond the Tradeoff: Dynamic Selectivity in Ionic Transport and Current Rectification. *J. Phys. Chem. B* **2019**, *123*, 1171–1185.

46. Decker, R.; Wang, Y.; Brar, V. W.; Regan, W.; Tsai, H. Z.; Wu, Q.; Gannett, W.; Zettl, A.; Crommie, M. F. Local Electronic Properties of Graphene on a BN Substrate *via* Scanning Tunnelling Microscopy. *Nano Lett.* **2011**, *11*, 2291–2295.

47. Zhu, Y.; Murali, S.; Cai, W.; Li, X.; Suk, J. W.; Potts, J. R.; Ruoff, R. S. Graphene

and Graphene Oxide: Synthesis, Properties, and Applications. *Adv. Mater.* **2010**, *22*, 3906–3924.

48. Gao, M.; Pan, Y.; Zhang, C.; Hu, H.; Yang, R.; Lu, H.; Cai, J.; Du, S.; Liu, F.; Gao, H. J. Tunable Interfacial Properties of Epitaxial Graphene on Metal Substrates. *Appl. Phys. Lett.* **2010**, *96*, 1–4.

49. Purcell, S. T.; Bocquet, L.; Siria, A.; Biance, A.-L.; Poncharal, P.; Fulcrand, R.; Blase, X. Giant Osmotic Energy Conversion Measured in a Single Transmembrane Boron Nitride Nanotube. *Nature* **2013**, *494*, 455–458.

50. Dash, S.; Patel, S.; Mishra, B. K. Oxidation by Permanganate: Synthetic and Mechanistic Aspects. *Tetrahedron* **2009**, *65*, 707–739.

51. Burton, O. J.; Babenko, V.; Veigang-Radulescu, V. P.; Brennan, B.; Pollard, A. J.; Hofmann, S. The Role and Control of Residual Bulk Oxygen in the Catalytic Growth of 2D Materials. *J. Phys. Chem. C* **2019**, *123*, 16257–16267.

52. Caneva, S.; Weatherup, R. S.; Bayer, B. C.; Blume, R.; Cabrero-Vilatela, A.; Braeuninger-Weimer, P.; Martin, M. B.; Wang, R.; Baehtz, C.; Schloegl, R.; Meyer, J. C.; Hofmann, S. Controlling Catalyst Bulk Reservoir Effects for Monolayer Hexagonal Boron Nitride CVD. *Nano Lett.* **2016**, *16*, 1250–1261.

53. Gao, L.; Ren, W.; Xu, H.; Jin, L.; Wang, Z.; Ma, T.; Ma, L. P.; Zhang, Z.; Fu, Q.; Peng, L. M.; Bao, X.; Cheng, H. M. Repeated Growth and Bubbling Transfer of Graphene with Millimetre-Size Single-Crystal Grains Using Platinum. *Nat. Commun.* **2012**, *3*, 697–699.

54. Shao, X. M.; Feldman, J. L. Micro-Agar Salt Bridge in Patch-Clamp Electrode Holder Stabilizes Electrode Potentials. *J. Neurosci. Meth.* **2007**, *159*, 108–115.

For Table of Contents Only